Journal of Power Sources 394 (2018) 140–147

Contents lists available at ScienceDirect

Journal of Power Sources

journal homepage: www.elsevier.com/locate/jpowsour

Extraordinary supercapacitance in activated carbon produced via a sustainable approach

Uttam Kumar, Vaibhav Gaikwad, Mohannad Mayyas, Veena Sahajwalla*, Rakesh K. Joshi**

Centre for Sustainable Materials Research and Technology (SMaRT@UNSW), School of Materials Science and Engineering, UNSW Sydney, NSW 2052, Australia

HIGHLIGHTS

- High quality porous activated carbons were prepared by physical activation process.
- Plastics from the end-of-life printers were used as the raw material.
- A maximum specific capacitance of around 220 F/g was obtained at 5 mV/s.
- The activated carbons exhibit high surface areas along with micro and mesopores.

GRAPHICAL ABSTRACT

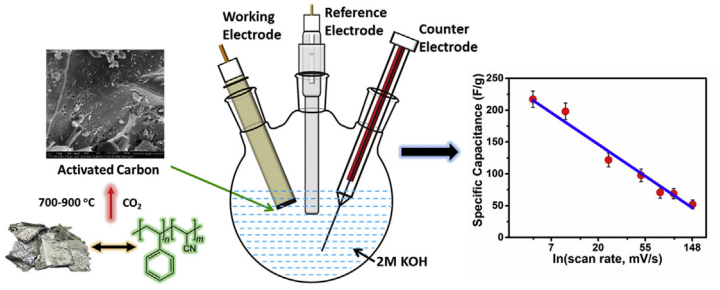

ARTICLE INFO

Keywords:
Sustainability
Activated carbon
Energy storage
Supercapacitance

ABSTRACT

Supercapacitors, with their high power density and quick charge/discharge capability, have gained attention as the highly desirable energy storage devices. Recent studies have shown that carbon-based materials with high surface area have huge potential for energy storage applications. It will be interesting if such carbon materials can be produced with desirable characteristics using a green approach. Herein, we report a highly reproducible sustainable approach of producing high surface area activated carbons directly from styrene acrylonitrile (SAN) plastics, obtained from the end-of-life printers. Activated carbons had high specific surface area and pore volume due to the mesopores and micropores generated in the carbon skeleton during the activation process, thus making these activated carbons a good potential candidate for supercapacitor electrode fabrication. We have studied the supercapacitance performance of these activated carbons with varied surface areas by conducting electrochemical experiments using a three-electrode system, with 2 M KOH as electrolyte, at scan rates ranging from 5 to 150 mV/s. While being used as a supercapacitor electrode without the addition of any conductive additives such as carbon black, specific gravimetric capacitance values of as high as 220 F/g were achieved. This is an outstanding supercapacitance performance of carbons produced using waste resources.

1. Introduction

The ever-increasing demand for energy has led the researchers around the world to develop advanced energy storage systems. Supercapacitors are a type of energy-storage devices that store energy either by electrochemical double layer capacitance (EDLC) which stores the charge electrostatically using reversible adsorption of electrolyte ions onto porous electrode materials with high ion-accessible surface area or pseudocapacitance which involves the fast Faradaic surface redox reactions [1–3]. These two charge storage mechanisms work concurrently when a potential difference is present between the two electrodes [4]. The supercapacitors have gained a particular attention

* Corresponding author.
** Corresponding author.
E-mail addresses: veena@unsw.edu.au (V. Sahajwalla), r.joshi@unsw.edu.au (R.K. Joshi).

https://doi.org/10.1016/j.jpowsour.2018.05.054
Received 17 February 2018; Received in revised form 9 May 2018; Accepted 14 May 2018
Available online 26 May 2018
0378-7753/ © 2018 Elsevier B.V. All rights reserved.

due to their high power density, long cycle life, excellent electrochemical stability, and quick charge/discharge capability [5,6]. Owing to these excellent properties, the supercapacitors could potentially be used in energy storage applications such as hybrid electric vehicles, renewable energy, consumer electronics, industrial equipment, implantable biocompatible electronic medical devices, emergency doors, and large-scale grid storage [7–12]. Various types of carbons, such as graphene, carbon nanotubes, nanotemplates, activated carbons, carbon nanofibers, etc., have been investigated to be used as electrodes for supercapacitors [13–17]. For instance, Xia et al. [18] used three-dimensional porous graphene-like sheets and achieved a capacitance of 91.15 F/g. However, activated carbons have been the material of choice for the supercapacitor electrode fabrication mainly due to their low cost, high specific surface area, good stability, and high conductivity [19,20].

Carbon-rich precursors can be converted to the activated carbon using physical or chemical activation process. Physical activation involves the carbonisation of the carbon precursor in an inert atmosphere at temperatures in the range of 600–900 °C, followed by the selective oxidation in CO_2 or steam at 350–1000 °C, to develop the porous structure within carbon skeleton [21,22]. In the chemical activation process, the carbon precursor is impregnated with an activating agent prior to the carbonisation at 450–900 °C [23,24]. The conventional carbon sources such as coal, pitch, and petroleum coke have been heavily used as precursors to produce activated carbons [22]. The increased environmental awareness regarding the harmful impacts of the excessive use of fossil fuels has directed the research into exploring the alternative carbon precursors for the sustainable production of activated carbon. Various types of biomasses and waste streams have been used to synthesize activated carbon for EDLC applications [25–29].

Concerns about the declining reserves of natural resources and increasing levels of electronic waste volumes have accelerated the advances towards the recycling of e-waste. In 2014, an estimated 41.8 million tonnes of e-waste was generated globally, which constituted of approximately 8.6 million tonnes of plastics with a projected value of $15 billion [30]. Several studies have been carried out to use this ever-growing stream of e-waste plastics into various value-added applications such as clean fuel production, filler for thermosetting and thermoplastic resin matrix composites, and energy recovery among many others [31–33]. Conversion of these waste plastics to the activated carbons with high surface area represents a suitable method to produce feedstock materials which are particularly useful in supercapacitor applications.

Herein, we developed a streamlined process to synthesize meso-microporous activated carbons (ACs), by the thermal transformation of styrene acrylonitrile (SAN) plastics retrieved from end-of-life printers, to be used in the fabrication of supercapacitor electrodes for energy storage applications. The as-obtained carbons after the physical activation were examined as electrode materials in a three-electrode cell with a 2 M KOH electrolyte, without any further treatment or addition of a conductive additive such as carbon black. These activated carbons displayed excellent electrochemical performance. The activated carbon synthesized at 900 °C reached the specific gravimetric capacitance of around 220 F/g. A detailed characterization of the activated carbons was performed to establish a correlation between their properties and electrochemical performance. Utilization of e-waste plastics for supercapacitor applications will not only help in diverting the e-waste plastics from the landfills, thus avoiding the harmful impacts of this waste stream on the environment, but also it will provide energy storage industry with a relatively greener precursor material for the supercapacitor electrode fabrication.

2. Experimental

2.1. Materials

Styrene Acrylonitrile (SAN) is widely used in the outer casing of electronic devices. The SAN plastic sample used in this study came from the end-of-life printers and it was supplied to us by an electronic waste management company TES-AMM Pty Ltd. To ensure the type of plastics under study, a Fourier transform infrared (FTIR) spectrum was obtained, in our earlier published work [34]. The spectrum for these waste plastics aligned perfectly with the spectrum for the standard poly (styrene acrylonitrile), including the characteristic peaks for the styrene ring stretching at 1453 and the -CN group stretching at 2237 cm^{-1}. Nafion perfluorinated resin solution (5% in lower aliphatic alcohols and water, contains 15–20% water) was used as a binder in electrode fabrication and was purchased from Sigma-Aldrich (Product ID. 274704 ALDRICH). Potassium hydroxide pellets used in the electrolyte preparation were purchased from Chem-Supply Pty Ltd. For this study, all percentages are presented as weight %, unless specified otherwise.

2.2. Synthesis of meso-microporous activated carbon

Physical activation method was employed to produce activated carbons from the plastic material under study. Carbonisation experiments were performed at the temperatures 700, 800, and 900 °C for the preparation of carbonaceous solid residue from SAN plastics. These experiments were performed in a horizontal tubular furnace and an inert atmosphere was created inside the furnace by pumping the N_2 gas at a flow rate of 1 L/min. The schematic and the set-up of the furnace is described in detail in our earlier publication [35,36]. One gram of pulverized SAN plastic was placed in an alumina crucible which was inserted in the preheated furnace using a graphite rod. It stayed in the hot zone of the furnace for 15 min. The yield of the carbonised solid residue was ~5% at all the heat treatment temperatures used in this study. The residue thus obtained was ground into a fine powder using a pestle and mortar.

The activation of the carbonised solid residue was performed using CO_2 as the oxidizing agent. Solid residue obtained after carbonisation was placed in the horizontal tubular furnace under inert atmosphere created by N_2 gas which was switched to the CO_2 atmosphere (flow rate, 1 L/min) before the sample was transferred to the hot zone of the furnace. The solid residues obtained at 700, 800, and 900 °C were activated for 3 h at the temperatures of 700, 800, and 900 °C respectively. The activated carbon (AC) samples were cooled down under inert N_2 atmosphere. The obtained ACs were designated as S700, S800, and S900; 'S' being the SAN-derived AC and 700, 800, and 900 representing the temperature. A weight loss of ~14% occurred during the activation process at all the activation temperatures used in this study. After the physical activation, the ACs were used as the electrode material without any post-treatment.

2.3. Characterization of activated carbons

The ACs were characterized using various analytical tools. Brunauer-Emmett-Teller (BET) surface area analysis (Micrometrics TriStar 3000 analyzer) was used to perform N_2 adsorption/desorption measurements to obtain specific surface area (S_{BET}), pore-size distribution, and total pore volume (V_T) of the ACs. Before the analysis, the samples were degassed, and vacuum dried for at least 3 h at 150 °C. The Barrette-Joynere-Halenda (BJH) method was used to calculate the mesopore surface area, pore volume, and pore size. X-ray photoelectron spectroscopy (XPS, Thermo Scientific, UK) was performed to observe the chemical state of the carbon present in ACs. ESCALAB 250Xi XPS spectrometer with a monochromated Al Kα as the X-ray source (energy 1486.68 eV) was used for this analysis. XPS chamber was operated at ultra-high vacuum (~2×10^{-9} mbar). The adventitious carbon C1s

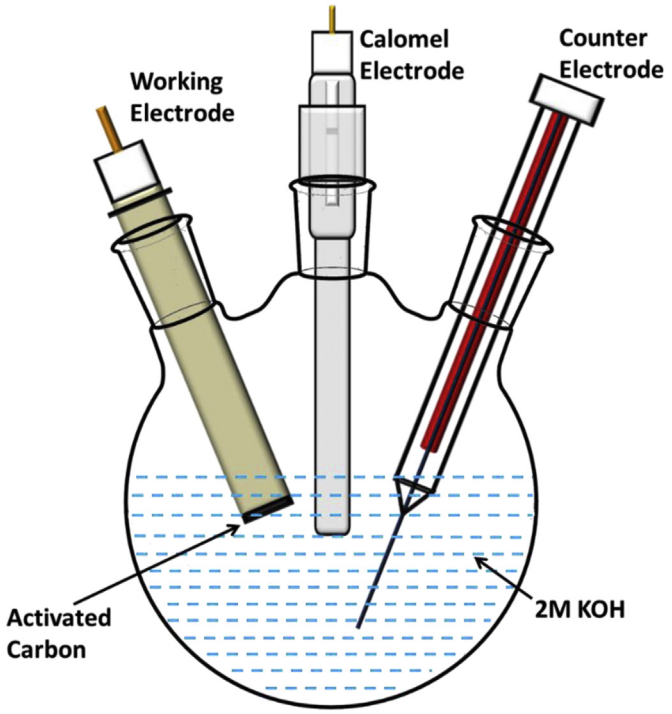

Fig. 1. Schematic of the three-electrode cell system used in the present study for electrochemical measurements.

peak at 284.8 eV was set as the reference binding energy. For the improved detection sensitivity, the analysis was done at photoelectron take-off angle of 90°. Renishaw inVia Raman Microscope was used with 532 nm Argon Ion Laser to acquire Raman spectrum. The spectrum was recorded over the range of 2000–700 cm^{-1}. Scanning electron microscopy (SEM, Nova NanoSEM 230) was used to obtain ultra-high imaging resolution of the morphology of the ACs.

2.4. Electrochemical measurements

Electrochemical performance of the ACs was investigated using cyclic voltammetry (CV) and electrochemical impedance spectroscopy (EIS). Biologic VSP 300 electrochemical workstation, with a three-electrode cell (schematic shown in Fig. 1), was employed to carry out these measurements.

A saturated calomel electrode (SCE) was used as the reference electrode and platinum wire as the counter electrode. The sample for the electrochemical measurements was prepared by mixing 2 mg of AC sample with 20 µL of Nafion perfluorinated resin solution. The sample paste thus prepared was pasted on the platinum electrode which was then used as a working electrode. 2 M aqueous KOH solution, which was prepared using KOH pellets and distilled water, was used as the electrolyte. CV experiments were performed at the scan rates ranging between 5 and 150 mV/s in the potential window of −1.5 to +1.5 V. The following equation (1) was used to calculate the specific gravimetric capacitance (C, F/g) of the ACs from the CV curves:

$$C = \frac{Area\ under\ the\ CV\ curve\ (mA.\ V)}{2\ x\ scan\ rate\ (mV/s)\ x\ potential\ window\ (V)\ x\ mass\ of\ the\ AC\ (g)} \quad (1)$$

As 2 mg of AC was used in all the experiments, the value of the mass of the AC will be 0.002 g in all the calculations. Potential window value will be 3.0 V.

3. Results and discussion

3.1. BET surface area analyses

The EDLC performance depends greatly on the electrode materials' specific surface area, pore volume, and pore size distribution. Hence, nitrogen adsorption/desorption experiments were performed on the ACs prepared through physical activation. The corresponding isotherms and pore size distributions are as shown in Fig. 2. All the nitrogen adsorption/desorption isotherms are 'type I' isotherms as exhibited by the steep rise in adsorbed volume of N_2 at , suggesting the high level of microporosity [37]. Table 1 summarizes the specific surface area, pore volume, and average pore sizes where V_{ads} is the BJH adsorption cumulative volume and V_{des} is the BJH desorption cumulative volume of pores between 1.7 and 300 nm diameter; d_{ads} and d_{des} are the average pore diameters for BJH adsorption and desorption, respectively. According to IUPAC classification, micropores are < 2 nm, mesopores are 2–50 nm in diameter, and macropores are > 50 nm. The carbon materials with regularly interconnected mesopores (with micropores on the mesopores walls) and high specific surface area are materials of choice for EDLC electrodes [38]. S700 and S800 showed very similar nitrogen adsorption/desorption isotherms and pore size distribution which is also evident from the obtained S_{BET}, pore volume, and average pore size values. However, the S_{BET} value increased from 496.96 m^2/g for S700 to 1357.82 m^2/g for S900 samples. During the activation process, the active oxygen in CO_2 opens up the pores by burning the carbonisation off-products trapped in the pores [21]. The higher specific surface area value for S900 may possibly be due to the higher activation temperature employed for the preparation of S900. It can also be noted that pore volume also increased from approximately 0.1 cm^3/g for S700 and S800 to around 0.2 cm^3/g for S900 further indicating the larger porosity development in S900 sample. Average pore size decreased from ~5.5 nm for S700 to ~4.1 nm for S900 sample. This observation is also evident from the pore size distribution and indicates the presence of larger number of micropores in S900 samples which may have resulted in higher surface area for S900. Although there is no clear correlation between the specific surface area and specific capacitance, various researchers have found that increased specific surface area generally enhances the ability of carbon materials to store the charge at the electrode/electrolyte interface. Recent studies suggest that pore size distribution of carbon nanostructures play a more important role towards the capacitance enhancement than the specific surface area [20]. For instance, activated carbon prepared from bamboo with S_{BET} value of 1250 m^2/g had a specific capacitance of 65 F/g whereas activated carbon from natural flax with a S_{BET} value of 645 m^2/g showed a specific capacitance of 325.8 F/g [22,39]. Moreover the capacitance has been reported to increase with the decrease in pore width, however, the micropores smaller than 0.5 nm are hardly accessible to electrolyte ions and may not contribute towards charge storage [40]. Based on the BET measurements, S900 sample has the highest specific surface area and pore volume and thus more extensive porous structure.

3.2. X-ray photoelectron spectroscopy

The surface chemical composition of synthesized ACs was examined by XPS. The typical features observed for the activated carbon samples are illustrated in Table 2. The elements identified by XPS on the surface of the samples are C, O, N, P, and Ti. The detected Ti may originate from TiO_2 which is generally added to the plastics as a pigment. C1s peaks, fitted with multiple components, are shown in Fig. 2(c, d, and e). Survey scan for S900 is represented in Fig. 2(f) and has the peaks for C1s and O1s at the binding energy values of 284.5 and 532.2 eV, respectively. The high-resolution XPS spectrum of C1s was deconvoluted into three different peaks at around 284.8, 286.1, and 287.2 eV which can be attributed to $C-C/C-H$, $C-O$, and $C=O$, respectively [41,42]. An atomic concentration of 9.64, 3.32, and 8.24% for C1s B

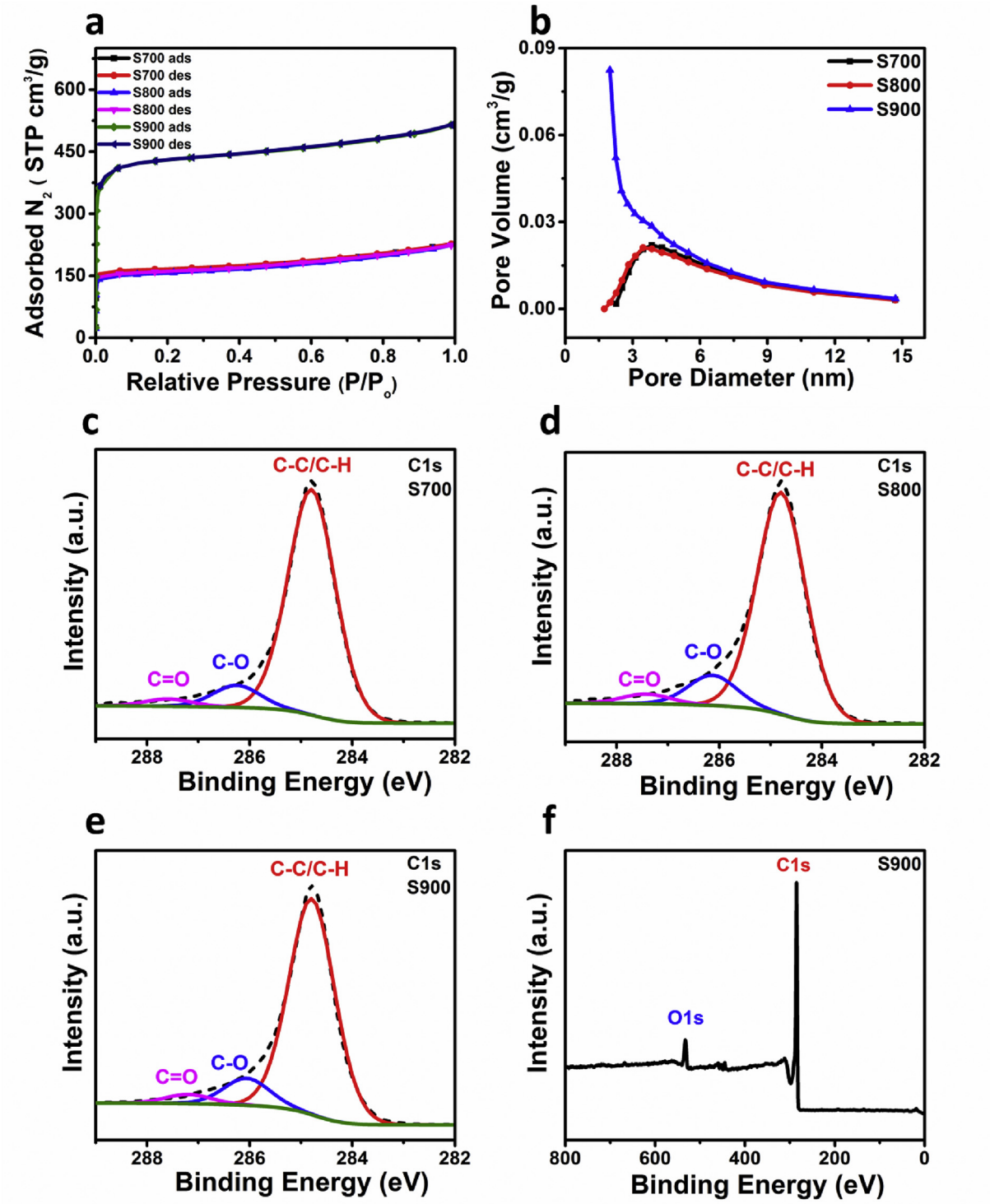

Fig. 2. (a) N_2 adsorption/desorption isotherms, (b) corresponding pore size distribution for the activated carbons; deconvoluted XPS C1s peaks for the activated carbon synthesized at (c) 700 °C, (d) 800 °C, (e) 900 °C, and (f) XPS survey scan peaks for the S900 sample. The green line in figures (c, d, and e) represents the background. (For interpretation of the references to colour in this figure legend, the reader is referred to the Web version of this article.)

($C-O$), C1s C ($C=O$) and O1s in S900 indicates the significant presence of oxygen functional groups. The presence of oxygen-containing surface functionalities can lead to increased specific capacitance and amount of energy stored due to pseudocapacitance effects and/or the improved wettability of the carbon electrode resulting in improved pore access [21,40]. A comparatively higher atomic concentration of oxygen-containing surface functionalities in S900 sample may contribute towards higher specific capacitance when this sample is used as an electrode.

3.3. Raman spectroscopy

Raman spectroscopy was used to obtain the information on the chemical structure of the activated carbons. Raman spectra were acquired in the wavenumber range of 700–2000 cm^{-1} and are displayed in Fig. 3(a). Two distinct peaks can be seen for all the activated carbons

Table 1
BET surface area measurements and pore characteristics for the synthesized activated carbons.

Sample	S_{BET} (m^2/g)	Pore Volume (cm^3/g)		Pore Size (nm)	
		V_{ads}	V_{des}	d_{ads}	d_{des}
S700	496.96	0.131	0.113	5.46	5.52
S800	489.92	0.129	0.121	5.25	5.28
S900	1357.82	0.194	0.191	4.07	4.11

Table 2
Peak positions of fitted XPS peaks for the S700, S800, and S900 sample.

Name	S700		S800		S900	
	Peak BE (eV)	Atomic %	Peak BE (eV)	Atomic %	Peak BE (eV)	Atomic %
C1s A	284.79	82.67	284.79	74.88	284.79	77.21
C1s B	286.25	8.12	286.13	10.23	286.06	9.64
C1s C	287.59	2.72	287.43	3.3	287.19	3.32
O1s	532.65	5.36	533.88	7.53	532.68	8.24

at ~1340 (D-band) and ~1590 cm^{-1} (G-band). Disorder-induced D band corresponds to the extent of disorder in the structure and G band corresponds to the E_{2g} vibrations and sp^2 hybridized carbon [43]. The ratio of the intensities of D and G bands (I_D/I_G) has been widely used to obtain the degree of organization and graphitization in carbon materials [44]. An intense and broad D-band peak indicates poorly ordered carbon. In the present study, for all the 3 samples, the intensity of D band was found to be comparable to G band which suggests high degree of disorder in the structure. The I_D/I_G ratio was calculated to be 0.95, 0.99, and 1.06 for S700, S800, and S900, respectively. An increase in the $I_D/I_G$is normally attributed to the increased disorder in the structure which indicates that S900 sample has the most disordered chemical structure. Activation process forms the micropores in the carbon framework, thus leading to increased number of defects and a larger I_D/I_G value [45]. A higher value of I_D/I_G for S900 can be explained by higher activation temperature, as higher temperature of activation may introduce more micropores as compared to the activation at lower temperature. Raman spectra were curve fitted using Gaussian function to calculate the full width at half maximum (FWHM) values for G-band. The FWHM value for G-band for S900 sample was found to be 87 cm^{-1} which is much higher than the FWHM value (15-23 cm^{-1}) for highly ordered pyrolytic graphite [46]. This further indicates the low degree of order in the structure for the ACs. The findings of Raman analysis can be strengthened by the BET surface area analysis where S900 sample was found to have the highest value of BET surface area.

3.4. Scanning electron microscopy

SEM analysis was performed on the S900 sample and the corresponding images of the two different surface morphologies observed are shown in Fig. 3(b) and (c). Surface morphology of the electrode material plays an important role in the charge storage phenomena. The images obtained clearly show the mesopores and macropores present in the sample and justify the high specific surface area and high pore volume obtained for the S900 sample. Furthermore, the pore size distribution for S900 indicated the presence of a large number of micropores which may have contributed to the high specific surface area value for S900. These micropores are perhaps drilled on the mesopore walls as observed by other researchers [47]. These interconnected pore channels help in ion transport across the bulk of the carbon and thus enhance the ion-accessible surface area. Larger diameter mesopores facilitate electrolyte penetration and ion transportation at low resistance. Additionally, due to the smaller size, micropores greatly enhance the specific surface area to provide more sites for charge storage.

3.5. Electrochemical analysis

Owing to its meso-microporous structure and high specific surface area, the activated carbons synthesized in the present study are expected to be a promising candidate for supercapacitor applications as an electrode material. There are two major charge storage mechanisms (EDLC and pseudocapacitance) and both work simultaneously depending on the surface area, materials, and the voltage applied between the electrodes. The cyclic voltammetry (CV) curves of the ACs and the capacitance values calculated from the CV curves using equation (1) are shown in Fig. 4. It can be clearly seen that for a given scan rate, the sample S900 exhibits higher current densities and larger stored charge (i.e., area under CV curve) compared to S700 and S800. In all the samples, the capacitance values were observed to decrease significantly with increasing the scan rate as shown in Fig. 4(d). For instance, for S700 sample, the capacitance dropped from 55 F/g to 3.5 F/g when scan rate was increased from 5 mV/s to 150 mV/s. At lower scan rates, the electrolyte ions have adequate time to infiltrate into the pores of the ACs, whereas at higher scan rates, the ions accumulate only on the

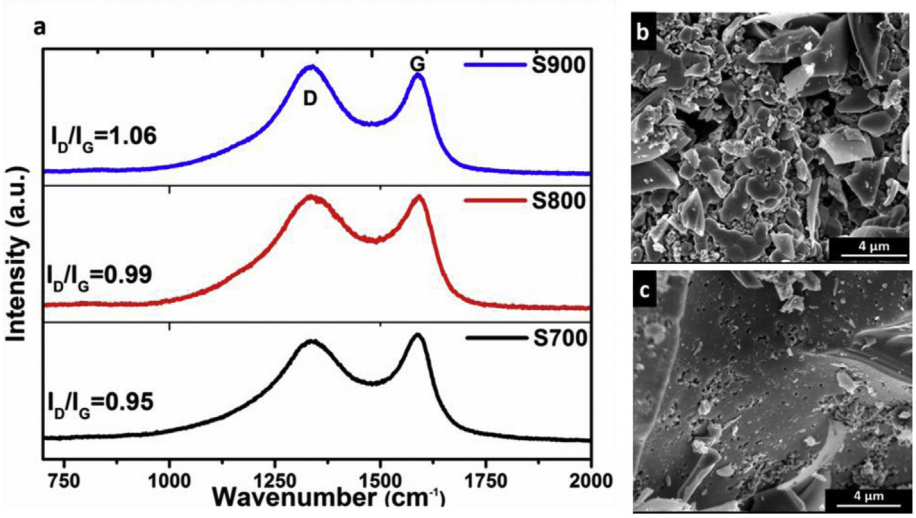

Fig. 3. (a) Raman spectra (acquired using 532 nm Argon Ion Laser) of the activated carbons prepared at 700, 800, and 900 °C, and (b), (c) SEM image (obtained using Nova NanoSEM 230) of activated carbon synthesized at 900 °C.

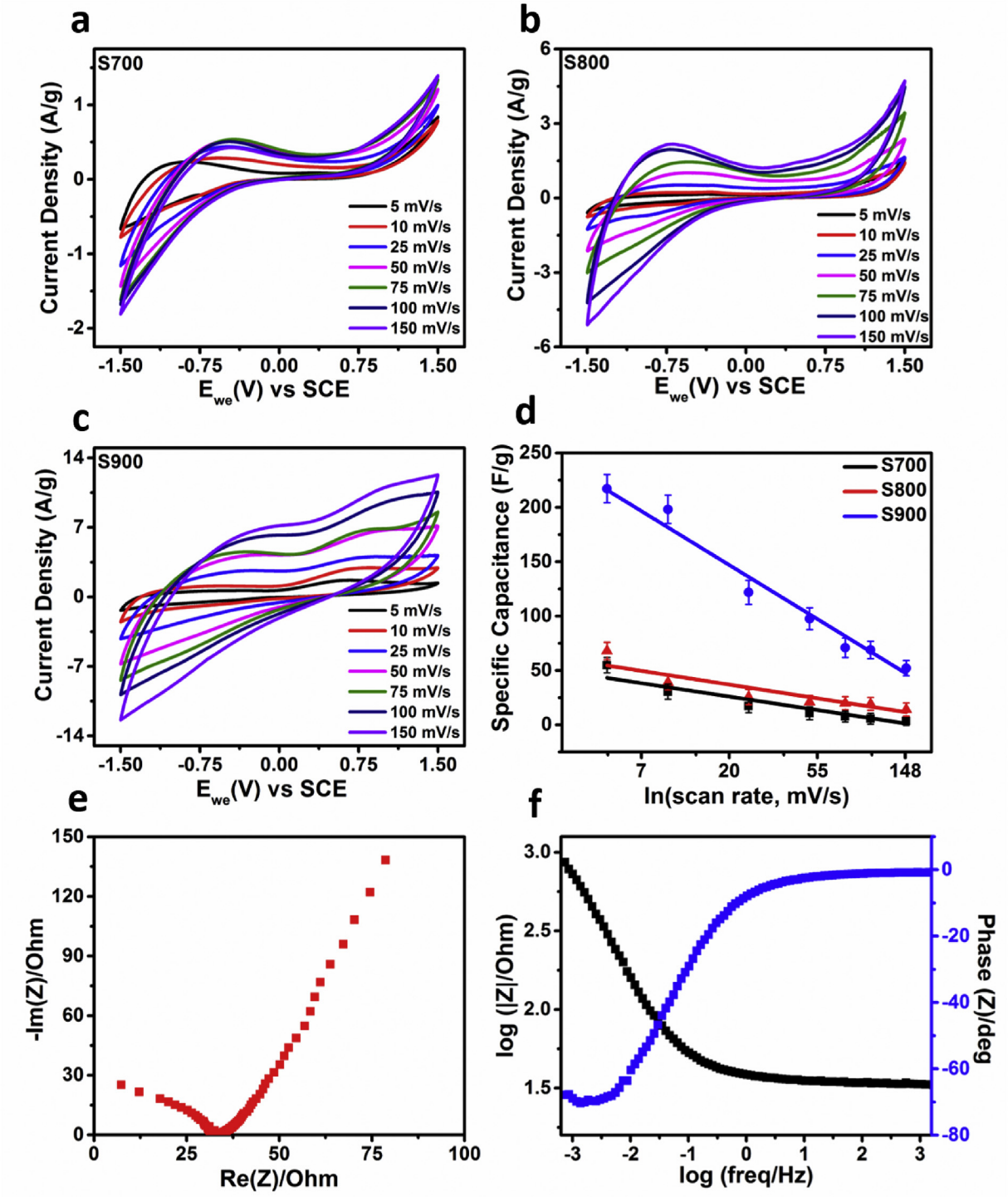

Fig. 4. Electrochemical performance of SAN-derived activated carbons from experiments carried out with a three-electrode cell. CV curves for (a) S700, (b) S800, and (c) S800; (d) specific capacitance trends with the variation in scan rate; (e) Nyquist plot for S900 sample; (f) bode impedance plot for S900 sample.

outer surface due to sluggish ion diffusion [48]. For that reason, higher scan rates result in lower capacitance value. Additionally, the S700 and S800 samples exhibited quite comparable capacitance values which can be attributed to both the samples having very similar values of the specific surface area, pore volume, and pore size distribution as shown in Table 1. The highest value of capacitance obtained in this study was 217 F/g for the S900 sample at 5 mV/s. The superior capacitance of S900 can be attributed to its higher specific surface area (S_{BET}) value of 1358 m^2/g which is much higher as compared to S700 and S800. Due to the higher S_{BET} value and larger pore volume, S900 sample has more ion-accessible trap sites, thus facilitating the high-charge storage capability through faster electrolyte transportation and ion diffusion [49].

The electrochemical performance of the ACs was further studied by performing electrochemical impedance spectroscopy (EIS). Based on the CV measurements, S900 was found to exhibit the highest capacitance and thus S900 was selected as the ideal candidate for further analysis. For S900, EIS Nyquist and the bode impedance plots are shown in Fig. 4(e) and (f), respectively. The Nyquist plot shows an incomplete semicircle at high frequency and a vertical linear feature at mid and low frequencies. The semicircle feature has been reported for

many carbons [50] which may be ascribed to the charge transfer resistance at high frequencies in activated carbons. This high resistance may be attributed to oxygen-containing functional groups on the carbon surface and also to the fact that no conductive carbon was added during the electrode fabrication in the present study. In the middle frequency region where ion diffusion effects at the electrode/electrolyte interface are dominant, a diagonal line is observed with a slope of around 45°, which represents the warburg impedance [51]. The subsequent straight line in the low frequency region is related to the dominance of double-layer charge storage [50]. Considering that the electrode was fabricated without adding any type of conducting carbons, the S900 exhibits a relatively good conductivity. The bode plot, in Fig. 4(f), displays the frequency dependent impedance and the phase angle diagrams. At frequency range > 1 Hz, the impedance is at minimum and nearly constant. In the frequency range < 1 Hz, the impedance starts to increase with simultaneous increase in the phase shift, suggesting that at this frequency range, double-layer or charge accumulation starts to develop on the surface of the activated carbon. When the frequency is lower than 0.01 Hz, the phase angle diagram plateaus at phase angle around −70°. This value of phase shift means that the S900 at this frequency range exhibits a predominant capacitive behavior rather than a series resistance. The further increase in the impedance at frequency higher than 0.01 Hz is related to the diffusion layer resistance developed on the surface of S900.

4. Conclusions

We have investigated the use of styrene acrylonitrile (SAN) plastics retrieved from end-of-life printers as a source of activated carbon with potential use as an electrode material for supercapacitors. Three different activated carbon samples were successfully prepared using a green and effective strategy by physical activation in the CO_2 atmosphere at 700, 800, and 900 °C. The obtained activated carbons possessed a meso-microporous structure with BET specific surface areas of 497, 490, and 1358 m^2/g respectively. When applied as supercapacitor electrodes without the use of any conductive additives, these activated carbons exhibited excellent capacitance values in 2 M aqueous KOH electrolyte solution. S900 sample demonstrated best capacitive performance with a specific gravimetric capacitance value of ~220 F/g at a scan rate of 5 mV/s, showing great potential as a candidate for advanced electrode material in supercapacitor applications. This exceptional performance can be attributed to faster ion diffusion facilitated by the highly porous structure in the activated carbon synthesized and activated at 900 °C. Use of the SAN plastics as a feedstock for the generation of activated carbons will provide the energy storage industry with a relatively greener alternative material for the supercapacitor electrodes fabrication which may help in diverting the e-waste plastics from landfills and incinerators, thus enhancing the environmental sustainability.

Acknowledgements

The authors would like to acknowledge the support received through an Australian Government Research Training Program Scholarship and the technical support provided by the Mark Wainwright Analytical Centre staff at the University of New South Wales.

References

[1] M. Kim, I. Oh, J. Kim, Superior electric double layer capacitors using micro- and mesoporous silicon carbide sphere, J. Mater. Chem. 3 (2015) 3944–3951, http://dx.doi.org/10.1039/C4TA07110G.
[2] P. Simon, Y. Gogotsi, Materials for electrochemical capacitors, Nat. Mater. 7 (2008) 845–854, http://dx.doi.org/10.1038/nmat2297.
[3] J.-S.M. Lee, M.E. Briggs, C.-C. Hu, A.I. Cooper, Controlling electric double-layer capacitance and pseudocapacitance in heteroatom-doped carbons derived from hypercrosslinked microporous polymers, Nanomater. Energy 46 (2018) 277–289, http://dx.doi.org/10.1016/j.nanoen.2018.01.042.
[4] J. Wang, S.-P. Feng, Y. Yang, N.Y. Hau, M. Munro, E. Ferreira-Yang, G. Chen, "Thermal charging" phenomenon in electrical double layer capacitors, Nano Lett. 15 (2015) 5784–5790, http://dx.doi.org/10.1021/acs.nanolett.5b01761.
[5] A. Sanchez-Sanchez, M.T. Izquierdo, S. Mathieu, J. González-Álvarez, A. Celzard, V. Fierro, Outstanding electrochemical performance of highly N- and O-doped carbons derived from pine tannin, Green Chem. 19 (2017) 2653–2665, http://dx.doi.org/10.1039/C7GC00491E.
[6] J. Vatamanu, O. Borodin, M. Olguin, G. Yushin, D. Bedrov, Charge storage at the nanoscale: understanding the trends from the molecular scale perspective, J. Mater. Chem. 5 (2017) 21049–21076, http://dx.doi.org/10.1039/C7TA05153K.
[7] L.L. Zhang, X.S. Zhao, Carbon-based materials as supercapacitor electrodes, Chem. Soc. Rev. 38 (2009) 2520, http://dx.doi.org/10.1039/b813846j.
[8] X. Fan, G. Yang, X. Chen, X. He, X. Huang, L. Gao, Effect of carboxymethyl cellulose on the drying dynamics and thermal cracking performance of iron ore green pellets, Powder Technol. 267 (2014) 11–17, http://dx.doi.org/10.1016/j.powtec.2014.07.011.
[9] S. He, Y. Hu, J. Wan, Q. Gao, Y. Wang, S. Xie, L. Qiu, C. Wang, G. Zheng, B. Wang, H. Peng, Biocompatible carbon nanotube fibers for implantable supercapacitors, Carbon N. Y. 122 (2017) 162–167, http://dx.doi.org/10.1016/j.carbon.2017.06.053.
[10] Y. Gogotsi, P. Simon, True performance metrics in electrochemical energy storage, Science (80-.) 334 (2011) 917–918, http://dx.doi.org/10.1126/science.1213003.
[11] L. Wang, M. Huang, S. Chen, L. Kang, X. He, Z. Lei, F. Shi, H. Xu, Z.-H. Liu, δ-MnO 2 nanofiber/single-walled carbon nanotube hybrid film for all-solid-state flexible supercapacitors with high performance, J. Mater. Chem. 5 (2017) 19107–19115, http://dx.doi.org/10.1039/C7TA04712F.
[12] L. Weinstein, R. Dash, Supercapacitor carbons, Mater. Today 16 (2013) 356–357, http://dx.doi.org/10.1016/j.mattod.2013.09.005.
[13] A. Sanchez-Sanchez, A. Martinez de Yuso, F.L. Braghiroli, M.T. Izquierdo, E.D. Alvarez, E. Pérez-Cappe, Y. Mosqueda, V. Fierro, A. Celzard, Sugarcane molasses as a pseudocapacitive material for supercapacitors, RSC Adv. 6 (2016) 88826–88836, http://dx.doi.org/10.1039/C6RA16314A.
[14] C.W. Foster, M.P. Down, Y. Zhang, X. Ji, S.J. Rowley-Neale, G.C. Smith, P.J. Kelly, C.E. Banks, 3D printed graphene based energy storage devices, Sci. Rep. 7 (2017) 42233, http://dx.doi.org/10.1038/srep42233.
[15] A.S. Aricò, P. Bruce, B. Scrosati, J.-M. Tarascon, W. van Schalkwijk, Nanostructured materials for advanced energy conversion and storage devices, Nat. Mater. 4 (2005) 366–377, http://dx.doi.org/10.1038/nmat1368.
[16] Y. Bin Tan, J.-M. Lee, Graphene for supercapacitor applications, J. Mater. Chem. 1 (2013) 14814, http://dx.doi.org/10.1039/c3ta12193c.
[17] Z. Fan, J. Yan, L. Zhi, Q. Zhang, T. Wei, J. Feng, M. Zhang, W. Qian, F. Wei, A three-dimensional carbon nanotube/graphene sandwich and its application as electrode in supercapacitors, Adv. Mater. 22 (2010) 3723–3728, http://dx.doi.org/10.1002/adma.201001029.
[18] J. Xia, N. Zhang, S. Chong, D. Li, Y. Chen, C. Sun, Three-dimensional porous graphene-like sheets synthesized from biocarbon via low-temperature graphitization for a supercapacitor, Green Chem. (2018), http://dx.doi.org/10.1039/C7GC03426A.
[19] Z. Zhao, S. Hao, P. Hao, Y. Sang, A. Manivannan, N. Wu, H. Liu, Lignosulphonate-cellulose derived porous activated carbon for supercapacitor electrode, J. Mater. Chem. 3 (2015) 15049–15056, http://dx.doi.org/10.1039/C5TA02770E.
[20] F. Wang, X. Wu, X. Yuan, Z. Liu, Y. Zhang, L. Fu, Y. Zhu, Q. Zhou, Y. Wu, W. Huang, Latest advances in supercapacitors: from new electrode materials to novel device designs, Chem. Soc. Rev. 46 (2017) 6816–6854, http://dx.doi.org/10.1039/C7CS00205J.
[21] M. Sevilla, R. Mokaya, Energy storage applications of activated carbons: supercapacitors and hydrogen storage, Energy Environ. Sci. 7 (2014) 1250–1280, http://dx.doi.org/10.1039/C3EE43525C.
[22] L. Wei, G. Yushin, Nanostructured activated carbons from natural precursors for electrical double layer capacitors, Nanomater. Energy 1 (2012) 552–565, http://dx.doi.org/10.1016/j.nanoen.2012.05.002.
[23] N. Balahmar, A.S. Al-Jumialy, R. Mokaya, Biomass to porous carbon in one step: directly activated biomass for high performance CO 2 storage, J. Mater. Chem. 5 (2017) 12330–12339, http://dx.doi.org/10.1039/C7TA01722G.
[24] M. Sevilla, A.B. Fuertes, A green approach to high-performance supercapacitor electrodes: the chemical activation of hydrochar with potassium bicarbonate, ChemSusChem. 9 (2016) 1880–1888, http://dx.doi.org/10.1002/cssc.201600426.
[25] M.M. Pérez-Madrigal, M.G. Edo, C. Alemán, Powering the future: application of cellulose-based materials for supercapacitors, Green Chem. 18 (2016) 5930–5956, http://dx.doi.org/10.1039/C6GC02086K.
[26] X.-F. Tan, S. Liu, Y. Liu, Y.-L. Gu, G.-M. Zeng, X.-J. Hu, X. Wang, S.-H. Liu, L.-H. Jiang, Biochar as potential sustainable precursors for activated carbon production: multiple applications in environmental protection and energy storage, Bioresour. Technol. 227 (2017) 359–372, http://dx.doi.org/10.1016/j.biortech.2016.12.083.
[27] A.B. Fadhil, A.I. Ahmed, H.A. Salih, Production of liquid fuels and activated carbons from fish waste, Fuel 187 (2017) 435–445, http://dx.doi.org/10.1016/j.fuel.2016.09.064.
[28] M. Fujishige, I. Yoshida, Y. Toya, Y. Banba, K.-I. Oshida, Y.-S. Tanaka, P. Dulyaseree, W. Wongwiriyapan, K. Takeuchi, Preparation of activated carbon from bamboo-cellulose fiber and its use for EDLC electrode material, J. Environ. Chem. Eng. 5 (2017) 1801–1808, http://dx.doi.org/10.1016/j.jece.2017.03.011.
[29] Y. Gong, D. Li, C. Luo, Q. Fu, C. Pan, Highly porous graphitic biomass carbon as advanced electrode materials for supercapacitors, Green Chem. 19 (2017)

4132–4140, http://dx.doi.org/10.1039/C7GC01681F.
[30] A. Kumar, M. Holuszko, D.C.R. Espinosa, E-waste: an overview on generation, collection, legislation and recycling practices, Resour. Conserv. Recycl. 122 (2017) 32–42, http://dx.doi.org/10.1016/j.resconrec.2017.01.018.
[31] J. Guo, J. Guo, Z. Xu, Recycling of non-metallic fractions from waste printed circuit boards: a review, J. Hazard Mater. 168 (2009) 567–590, http://dx.doi.org/10.1016/j.jhazmat.2009.02.104.
[32] S.D. Anuar Sharuddin, F. Abnisa, W.M.A. Wan Daud, M.K. Aroua, Energy recovery from pyrolysis of plastic waste: study on non-recycled plastics (NRP) data as the real measure of plastic waste, Energy Convers. Manag. 148 (2017) 925–934, http://dx.doi.org/10.1016/j.enconman.2017.06.046.
[33] C. Ma, J. Yu, B. Wang, Z. Song, J. Xiang, S. Hu, S. Su, L. Sun, Chemical recycling of brominated flame retarded plastics from e-waste for clean fuels production: a review, Renew. Sustain. Energy Rev. 61 (2016) 433–450, http://dx.doi.org/10.1016/j.rser.2016.04.020.
[34] U. Kumar, V. Gaikwad, V. Sahajwalla, Transformation of waste toner to iron using e-waste plastics as a carbon resource, J. Clean. Prod. (2018), http://dx.doi.org/10.1016/j.jclepro.2018.05.010.
[35] U. Kumar, S. Maroufi, R. Rajarao, M. Mayyas, I. Mansuri, R.K. Joshi, V. Sahajwalla, Cleaner production of iron by using waste macadamia biomass as a carbon resource, J. Clean. Prod. 158 (2017) 218–224, http://dx.doi.org/10.1016/j.jclepro.2017.04.115.
[36] V. Gaikwad, U. Kumar, F. Pahlevani, A. Piadasa, V. Sahajwalla, Thermal transformation of waste toner powder into a value-added ferrous resource, ACS Sustain. Chem. Eng. 5 (2017) 11543–11550, http://dx.doi.org/10.1021/acssuschemeng.7b02875.
[37] L. Miao, D. Zhu, Y. Zhao, M. Liu, H. Duan, W. Xiong, Q. Zhu, L. Li, Y. Lv, L. Gan, Design of carbon materials with ultramicro-, supermicro- and mesopores using solvent- and self-template strategy for supercapacitors, Microporous Mesoporous Mater. 253 (2017) 1–9, http://dx.doi.org/10.1016/j.micromeso.2017.06.032.
[38] A.B. Fuertes, G. Lota, T.A. Centeno, E. Frackowiak, Templated mesoporous carbons for supercapacitor application, Electrochim. Acta 50 (2005) 2799–2805, http://dx.doi.org/10.1016/j.electacta.2004.11.027.
[39] D.A.G. Hegde, Activated carbon nanospheres derived from bio-waste materials for supercapacitor applications – a review, RSC Adv. 5 (2015) 88339–88352, http://dx.doi.org/10.1039/C5RA19392C.
[40] Y. Wang, Y. Song, Y. Xia, Electrochemical capacitors: mechanism, materials, systems, characterization and applications, Chem. Soc. Rev. 45 (2016) 5925–5950, http://dx.doi.org/10.1039/C5CS00580A.
[41] J. Zhang, W. Yang, J. Liu, Facile fabrication of supercapacitors with high rate capability using graphene/nickel foam electrode, Electrochim. Acta 209 (2016) 85–94, http://dx.doi.org/10.1016/j.electacta.2016.05.071.
[42] M. Varga, T. Izak, V. Vretenar, H. Kozak, J. Holovsky, A. Artemenko, M. Hulman, V. Skakalova, D.S. Lee, A. Kromka, Diamond/carbon nanotube composites: Raman, FTIR and XPS spectroscopic studies, Carbon N. Y. 111 (2017) 54–61, http://dx.doi.org/10.1016/j.carbon.2016.09.064.
[43] O. Mykhailiv, H. Zubyk, M.E. Plonska-Brzezinska, Carbon nano-onions: unique carbon nanostructures with fascinating properties and their potential applications, Inorg. Chim. Acta. 468 (2017) 49–66, http://dx.doi.org/10.1016/j.ica.2017.07.021.
[44] S. Dong, P. Alvarez, N. Paterson, D.R. Dugwell, R. Kandiyoti, Study on the effect of heat treatment and gasification on the carbon structure of coal chars and metallurgical cokes using fourier transform Raman spectroscopy, Energy Fuels 23 (2009) 1651–1661, http://dx.doi.org/10.1021/ef800961g.
[45] S. Xiong, J. Fan, Y. Wang, J. Zhu, J. Yu, Z. Hu, A facile template approach to nitrogen-doped hierarchical porous carbon nanospheres from polydopamine for high-performance supercapacitors, J. Mater. Chem. 5 (2017) 18242–18252, http://dx.doi.org/10.1039/C7TA05880B.
[46] O.O. Sonibare, T. Haeger, S.F. Foley, Structural characterization of Nigerian coals by X-ray diffraction, Raman and FTIR spectroscopy, Energy 35 (2010) 5347–5353, http://dx.doi.org/10.1016/j.energy.2010.07.025.
[47] H.-J. Liu, J. Wang, C.-X. Wang, Y.-Y. Xia, Ordered hierarchical mesoporous/microporous carbon derived from mesoporous titanium-carbide/carbon composites and its electrochemical performance in supercapacitor, Adv. Energy Mater. 1 (2011) 1101–1108, http://dx.doi.org/10.1002/aenm.201100255.
[48] T. Liu, F. Zhang, Y. Song, Y. Li, Revitalizing carbon supercapacitor electrodes with hierarchical porous structures, J. Mater. Chem. 5 (2017) 17705–17733, http://dx.doi.org/10.1039/C7TA05646J.
[49] J. Wang, J. Tang, B. Ding, V. Malgras, Z. Chang, X. Hao, Y. Wang, H. Dou, X. Zhang, Y. Yamauchi, Hierarchical porous carbons with layer-by-layer motif architectures from confined soft-template self-assembly in layered materials, Nat. Commun. 8 (2017) 15717, http://dx.doi.org/10.1038/ncomms15717.
[50] W. Qian, F. Sun, Y. Xu, L. Qiu, C. Liu, S. Wang, F. Yan, Human hair-derived carbon flakes for electrochemical supercapacitors, Energy Environ. Sci. 7 (2014) 379–386, http://dx.doi.org/10.1039/C3EE43111H.
[51] L. Lai, H. Yang, L. Wang, B.K. Teh, J. Zhong, H. Chou, L. Chen, W. Chen, Z. Shen, R.S. Ruoff, J. Lin, Preparation of supercapacitor electrodes through selection of graphene surface functionalities, ACS Nano 6 (2012) 5941–5951, http://dx.doi.org/10.1021/nn3008096.